ACS Photonics

Article

pubs.acs.org/journal/apchd5

Enhanced Magnetic and Electric Fields via Fano Resonances in Metasurfaces of Circular Clusters of Plasmonic Nanoparticles

Salvatore Campione,*,† Caner Guclu,*,† Regina Ragan,*,‡ and Filippo Capolino*,†

†Department of Electrical Engineering and Computer Science, University of California Irvine, Irvine, California 92697, United States

‡Department of Chemical Engineering and Materials Science, University of California Irvine, Irvine, California 92697, United States

ABSTRACT: We investigate for the first time the capacity of a two-dimensional periodic array (a metasurface) of circular nanoclusters (CNCs) of plasmonic nanoparticles to support *magnetic* Fano resonances. These resonances are characterized by narrow angular and/or spectral features in the reflection/transmission/absorption coefficients associated with a circular disposition of nanoparticles' dipole moments (forming a current loop) under oblique TE-polarized plane wave incidence illumination. We find that these narrow resonant features are either array-induced or single-CNC-induced, as shown by using a theoretical analysis based on the single dipole approximation and full-wave simulations, leading to enhanced magnetic and electric fields. In particular, array-induced resonances are narrower than single-CNC-induced ones and also provide even larger field enhancements, in particular generating a magnetic field enhancement of about 10-fold and an electric field enhancement of about 40-fold for a representative metasurface. We suggest that the novel results pertaining to metasurfaces made of CNCs shown here may be used for the development of sensors based on enhanced magnetic fields and for the enhancement of magnetic nonlinearities.

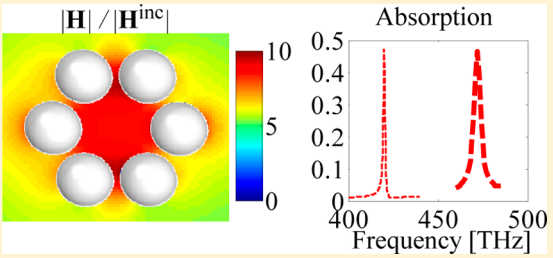

KEYWORDS: *metasurfaces, circular nanoclusters, Fano resonances, plasmonic nanoparticles*

Conventional materials in nature exhibit more commonly electric than magnetic response, the latter being particularly weak and even rare at terahertz and optical frequencies. This deficiency is at the foundation of the fervent quest for the development of artificial magnetism, which started with the use of split ring resonators[1−3] and then continued with the use of properly designed structures, either planar or three-dimensional.[4−14] Interestingly, collective plasmons (referred to as "magnetic plasmons" in ref 15) have enabled low-loss plasmonic waveguides and devices,[15] and magnetic resonances have been used for the development of sensors.[16] In this picture, the enhancement of magnetic fields, in addition to the enhancement of electric fields, has recently attracted a great deal of attention.[11,17−22] Among other structures, clusters of plasmonic nanoparticles have also been shown to contribute to boost such enhancements.[11,22] In particular, the physics in our paper involves the use of magnetic Fano resonances to achieve magnetic field enhancement, through a completely different process with respect to what shown in ref 22. Instead, the authors of ref 11 fabricated an *asymmetric nanoring* made of four nanoparticles (i.e., an *isolated metamolecule*, as it has been called there). The work in ref 11 shows that such a structure supports a strong magnetic response coupled to a broad electric resonance, presenting the first experimental observation of a "magnetic-based Fano resonance" at optical frequencies under transverse electric (TE)-polarized plane wave incidence. We recall that Fano resonances are supported in arrays of or isolated close-packed clusters of plasmonic nanoparticles,[23−27] and more details on the topic may be found in refs 28−30. Their applications are numerous and include the development of sensing devices.[31] In this paper we rather use a metasurface (i.e., a planar two-dimensional periodic array) made of *symmetric* circular nanoclusters (CNCs) of plasmonic nanoparticles that supports two kinds of *magnetic* Fano resonances, characterized by narrow (angular and/or spectral) features associated with a circular disposition of nanoparticles' dipole moments (forming a current loop). Instead of perturbing the symmetry of the structure as in ref 11 to boost the CNC's magnetic Fano resonance (whose effect is still present in our metasurface), we further achieve an additional magnetic Fano resonance with features sharper than the single-CNC-induced one. We show that this additional resonance is induced by array effects, and it leads to even larger field enhancements and has not been analyzed before. In particular, we present for the first time, to the authors' knowledge, the analytical investigation of enhanced magnetic and electric fields achievable in metasurfaces made of CNCs illustrated in Figure 1 in correspondence with magnetic Fano resonances excitable under TE oblique plane wave incidence. The presence of such resonances is verified by both analytical calculations and full-wave simulations. The analytical approach encompasses the use of the electric polarizability of nanoparticles under single dipole approximation (SDA) and Green's functions (GFs), which can be generalized for any stratified medium, and thus is able to accurately model fabricated multilayered substrates.

Received: November 19, 2013
Published: February 7, 2014

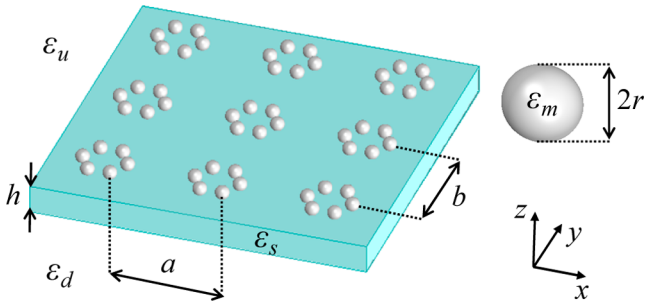

Figure 1. Metasurface of CNCs of plasmonic nanoparticles with relative permittivity ε_m and radius r on top of a layer with relative permittivity ε_s and thickness h. The medium where the particles are embedded and the one below the layer have relative permittivities ε_u and ε_d, respectively. Note that more complex multilayered substrates can be also considered.

Such metasurfaces may indeed be fabricated via self-assembly from colloidal solution, for example, integrating the chemical assembly process in ref 32 with ordered diblock copolymer surfaces.[33] The use of colloidal assembly to fabricate nanoparticle clusters in controlled geometries has been recently demonstrated.[34] While we consider spherical nanoparticles in this paper, similar properties can be achieved using other nanoparticle geometries, e.g., nanodisks. We stress that under TE incidence the nanoparticles are polarized only on the transverse plane; therefore disk-shaped nanoparticles could also be used for achieving sharp magnetic resonances. The description of the physics of a metasurface, combined with the account of substrate effects, is much more complex than that of an isolated metamolecule (as for example the one treated in ref 11) and is a required step for the development of innovative magnetic sensors and the improvement of magnetic nonlinearities.[35,36]

FORMULATION EMPLOYING 2D PERIODIC DYADIC GREEN'S FUNCTIONS

We briefly summarize the formulation based on two-dimensional periodic dyadic Green's functions that accounts for all the field contributions required to thoroughly describe the physics of a metasurface of nanoparticle clusters on top of a multilayered substrate.[37] The monochromatic time harmonic convention $\exp(-i\omega t)$ is implicitly assumed.

Consider the metasurface made of clusters of plasmonic nanoparticles (e.g., CNCs as in Figure 1) located at positions $\mathbf{r}_{i,mn} = \mathbf{r}_i + ma\hat{\mathbf{x}} + nb\hat{\mathbf{y}}$ on top of a multilayered substrate, where $\mathbf{r}_i = x_i\hat{\mathbf{x}} + y_i\hat{\mathbf{y}} + z_i\hat{\mathbf{z}}$, $i = 1, 2, ..., N$, with N being the number of particles in a unit cell, $m, n = 0, \pm1, \pm2, ...$, and a and b being the periods along the x and y directions, respectively. By resorting to the single dipole approximation,[38,39] valid when the electric dipolar term dominates the nanoparticle's scattered-field multipole expansion, the mnth particle in the array can be described by the electric dipole moment $\mathbf{p}_{i,mn} = \mathbf{p}_i \exp[i\mathbf{k}_B\cdot(\mathbf{r}_{i,mn} - \mathbf{r}_i)]$. In this equation, $\mathbf{k}_B = k_x\hat{\mathbf{x}} + k_y\hat{\mathbf{y}}$ is the Bloch wavevector, which also accounts for decay in case the wavenumbers are complex, and $\mathbf{p}_i$ is the electric dipole moment of the ith particle in a unit cell. (In general, more accurate results may be obtained by including multipolar field contributions.[38]) It is anticipated that the electric dipole moments $\mathbf{p}_i$ in a unit cell can collectively assume several dispositions (circular, linear, etc.): our main focus is on the circular disposition, signature of a strong magnetic resonance, and this will be better investigated in subsequent discussions.

The total electric field at a general position $\mathbf{r} = x\hat{\mathbf{x}} + y\hat{\mathbf{y}} + z\hat{\mathbf{z}}$ is given by

$$\mathbf{E}(\mathbf{r}, \mathbf{k}_B) = \mathbf{E}^{inc}(\mathbf{r}) + \mathbf{E}^{ref}(\mathbf{r}) + \sum_{i=1}^{N} \underline{\mathbf{G}}_{ml}^{\infty}(\mathbf{r}, \mathbf{r}_i, \mathbf{k}_B)\cdot\mathbf{p}_i \quad (1)$$

where $\mathbf{E}^{inc}$ is the incident electric field, $\mathbf{E}^{ref}$ is the portion of incident electric field reflected by the multilayered substrate, $\sum_{i=1}^{N} \underline{\mathbf{G}}_{ml}^{\infty}(\mathbf{r},\mathbf{r}_i,\mathbf{k}_B)\cdot\mathbf{p}_i$ is the field scattered by the metasurface including the effect of the multilayered substrate, and $\underline{\mathbf{G}}_{ml}^{\infty}$ represents the multilayered electric dyadic GF for the periodic phased array of electric dipoles that relates the induced electric dipole moment to the electric field. The term $\underline{\mathbf{G}}_{ml}^{\infty}$ is here computed by summing two terms as in ref 37 to guarantee fast convergence when evaluating fields at the array plane: (i) the periodic dyadic GF of an array of electric dipoles in homogeneous host medium computed through the Ewald method[40] and (ii) the periodic dyadic scattering GF computed through a spectral approach that takes into account the effect of the multilayered substrate. It is apparent that once the Green's function of a dipole in the multilayered environment is known, the dipole moments $\mathbf{p}_i$ are evaluated by solving the system for $i = 1, 2, ..., N$,

$$\sum_{j=1}^{N} \underline{\mathbf{A}}_{ij}\cdot\mathbf{p}_j = \alpha_{ee}[\mathbf{E}^{inc}(\mathbf{r}_i) + \mathbf{E}^{ref}(\mathbf{r}_i)] \quad (2)$$

with $\underline{\mathbf{A}}_{ij} = -\alpha_{ee}\underline{\mathbf{G}}_{ml}^{\infty}(\mathbf{r}_i, \mathbf{r}_j, \mathbf{k}_B)$ for $j \neq i$ and $\underline{\mathbf{A}}_{ii} = \underline{\mathbf{I}} - \alpha_{ee}\breve{\underline{\mathbf{G}}}_{ml}^{\infty}(\mathbf{r}_i, \mathbf{r}_i, \mathbf{k}_B)$, as previously described also in ref 40 for a homogeneous environment (the diacritical mark *breve* denotes regularized dyadic GF), where α_{ee} is the nanoparticle's electric polarizability (we use here the Mie expression[38]) and $\underline{\mathbf{I}}$ is the unit dyad. The total magnetic field can then be computed as

$$\mathbf{H}(\mathbf{r}, \mathbf{k}_B) = \mathbf{H}^{inc}(\mathbf{r}) + \mathbf{H}^{ref}(\mathbf{r}) + \sum_{i=1}^{N} \underline{\mathbf{G}}_{ml,H}^{\infty}(\mathbf{r}, \mathbf{r}_i, \mathbf{k}_B)\cdot\mathbf{p}_i \quad (3)$$

where $\mathbf{H}^{inc}$ is the incident magnetic field, $\mathbf{H}^{ref}$ is the portion of incident magnetic field reflected by the multilayered substrate, and $\underline{\mathbf{G}}_{ml,H}^{\infty}(\mathbf{r},\mathbf{r}_i,\mathbf{k}_B)$ is the multilayered magnetic dyadic GF for the periodic phased array of electric dipoles that relates the induced electric dipole moment to the magnetic field, computed in a similar manner to $\underline{\mathbf{G}}_{ml}^{\infty}(\mathbf{r}, \mathbf{r}_i, \mathbf{k}_B)$.

OPTICAL PROPERTIES OF A METASURFACE OF CIRCULAR NANOCLUSTERS UNDER OBLIQUE PLANE WAVE INCIDENCE

The electric dipole moments $\mathbf{p}_i$ computed by solving the system in eq 2 are used in this section to evaluate the optical properties of the metasurface, in particular absorption A, specular reflection R, and specular transmission T. We consider three representative multilayered substrate cases as in Figure 1 with the following parameters: (i) $\varepsilon_u = \varepsilon_d = \varepsilon_s = 1$ (array in homogeneous free space); (ii) $\varepsilon_u = \varepsilon_d = \varepsilon_s = 2.25$ (array in homogeneous silica SiO_2 environment); and (iii) $\varepsilon_u = \varepsilon_d = 1$ and $\varepsilon_s = 2.25$ with $h = 1000$ nm (array on top of a SiO_2 layer as illustrated in Figure 1). Nanoparticles are made of silver whose dielectric permittivity is modeled with experimental data including losses,[41] $r = 25$, $a = b = 300$ (in nm), and the gap between neighboring nanoparticles is 10 nm. We first consider

dx.doi.org/10.1021/ph4001313 | ACS Photonics 2014, 1, 254−260

TE-polarized incident plane waves with magnetic field in the plane of incidence, i.e., wavevector $\mathbf{k} = k_x\hat{\mathbf{x}} + k_z\hat{\mathbf{z}}$ and $\mathbf{E}^{inc}(\mathbf{r}) = E_y^{inc}\hat{\mathbf{y}}e^{i\mathbf{k}\cdot\mathbf{r}}$. Only TE waves with oblique incidence are expected to generate *magnetic* Fano resonances, as the magnetic field has a component along the z direction that excites the CNC of plasmonic nanoparticles and induces a circulating current, as it will be shown next. The absorption coefficient is computed following the optical theorem[38] as discussed in refs 42−44 by accounting for N nanoparticles in a unit cell as

$$A = \frac{-k}{|\mathbf{E}^{inc}|^2\varepsilon_0\varepsilon_u ab\cos\theta}\left[\mathrm{Im}(\alpha_{ee}^{-1}) + \frac{k^3}{6\pi\varepsilon_0\varepsilon_u}\right]\sum_{i=1}^{N}|\mathbf{p}_i|^2 \quad (4)$$

whereas reflection and transmission are computed following the formulation in ref 40. In eq 4, $k = k_0\sqrt{\varepsilon_u}$ is the wavenumber of the medium hosting the nanoparticles, k_0 is the free space wavenumber, and θ is the angle of incidence. Equation 4 is used because above certain angles nonspecular scattering is expected to appear due to higher order propagating Floquet harmonics, and thus A cannot be estimated through $1 - |R|^2 - |T|^2$.

For the three representative cases (i)−(iii) we show in Figure 2 the absorption coefficient evaluated as in eq 4 versus

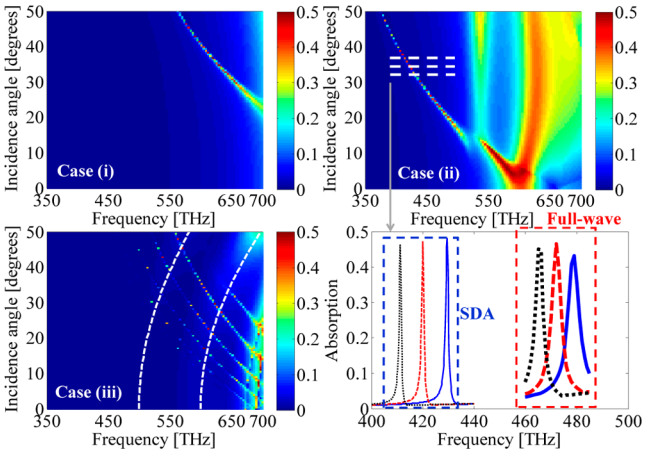

Figure 2. Absorption by the nanoparticles in a unit cell for a metasurface as in Figure 1 under TE plane wave incidence, evaluated using SDA, for three representative cases: (i) array in homogeneous free space; (ii) array in homogeneous SiO_2 environment; and (iii) array on top of a SiO_2 layer. Structural parameters are given in the text. For case (ii), we also report the comparison between SDA results (thin curves) and full-wave simulations (thick curves) for three angular cuts in the frequency range depicted by the three white dashed lines: 32.5 degrees (solid blue), 35 degrees (dashed red), and 37.5 degrees (dotted black).

frequency and angle of incidence when the array is illuminated by an oblique TE plane wave. For case (i), we observe the presence of a narrow magnetic resonance as a belt on incidence angle-frequency plane for incidence angles larger than 20 degrees in the frequency band 550−700 THz, which is due to array effects,[45,46] as it will be later shown. For case (ii), we observe a frequency shift toward lower frequencies of the resonant belt with respect to case (i), as expected by the increase of the host medium's dielectric constant. For example the feature in the 550−700 THz frequency band for case (i) moves to the 370−520 THz frequency band in case (ii). Other features with almost no angle dependence also appear for larger frequencies reported for case (ii) as vertical hotspots: the first one around 530 THz is associated with the magnetic resonance of the isolated CNC, and the second one is due to an electric quadrupole contribution. This fact will be better explained in the next section. Furthermore, for case (ii), we also performed full-wave simulations[47] for three constant-angle cuts versus frequency [depicted by the three white dashed lines in case (ii)], and in the same figure we plotted curves computed via SDA relative to the same cases. Besides a frequency shift attributed to multipolar effects (their presence will be shown in Section V), we observe a very good qualitative agreement: narrow resonances are observed with similar characteristics of strength and width, and full-wave simulations verify the SDA prediction that the resonance moves to lower frequencies for increasing angles of incidence. For case (iii), we observe the presence of several belts of narrow resonances instead of a single belt as observed in previous cases with homogeneous environments. Therefore we infer that the multilayered substrate can be optimized to obtain extra narrow resonances that can be used for sensing applications. We also observe that the substrate finite thickness results in the appearance of vague Fabry−Pérot features in the absorption map, where we superimpose dashed white lines denoting 2π-phase accumulation within the SiO_2 layer without the metasurface on top.

We consider now both TE- and transverse magnetic (TM)-polarized incident plane waves for the metasurface of case (ii) in Figure 2. The TM wave has the electric field in the plane of incidence: wavevector $\mathbf{k} = k_x\hat{\mathbf{x}} + k_z\hat{\mathbf{z}}$ and $\mathbf{E}^{inc}(\mathbf{r}) = E_0^{inc}(\cos\theta\hat{\mathbf{x}} - \sin\theta\hat{\mathbf{z}})e^{i\mathbf{k}\cdot\mathbf{r}}$. We show in Figure 3 the absorption coefficient, the

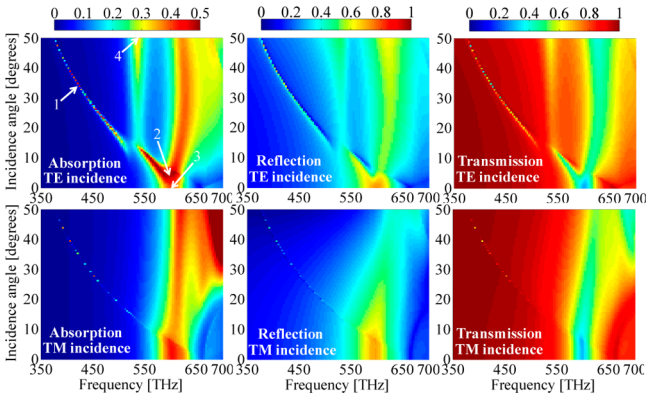

Figure 3. Absorption by the nanoparticles in a unit cell and magnitudes of specular reflection and transmission for the structure in case (ii) in Figure 2 by TE (top row) and TM (bottom row) incident plane waves. In the top-left panel, the white numbers indicate the setups analyzed in Section IV.

magnitude of specular reflection, and the magnitude of specular transmission versus frequency and angle of incidence. TE incidence is observed to generate narrow Fano resonances, much stronger than the ones appearing under TM incidence, as it will be clarified in the next section. Moreover, the narrow Fano resonances appearing in the frequency range 350−530 THz are array-induced, as it will be shown in the next section.

STRENGTHS OF ELECTRIC DIPOLE, MAGNETIC DIPOLE, AND ELECTRIC QUADRUPOLE

Our aim in this section is to understand the strengths of the electric dipole, magnetic dipole, and electric quadrupole representing the CNCs in multipolar expansion, investigating the same setup pertaining to the results in Figure 3. According

dx.doi.org/10.1021/ph4001313 | ACS Photonics 2014, 1, 254−260

to the definitions reported in Chapters 6 and 9 of ref 48 the electric (in [Cm]) and magnetic (in [Am^2]) dipoles and the electric quadrupole (in [Cm^2]) are, respectively, computed as

$$\mathbf{p} = \sum_{i=1}^{N} \mathbf{p}_i, \quad \mathbf{m} = \frac{-i\omega}{2} \sum_{i=1}^{N} \mathbf{r}_i \times \mathbf{p}_i, \quad \underline{\mathbf{Q}} = \sum_{i=1}^{N} [\mathbf{p}_i \mathbf{r}_i + \mathbf{r}_i \mathbf{p}_i] \tag{5}$$

We show in Figure 4 the magnitudes of the electric dipole $|\mathbf{p}|$ and of the magnetic dipole $|\mathbf{m}|$ and the norm-2 of the electric

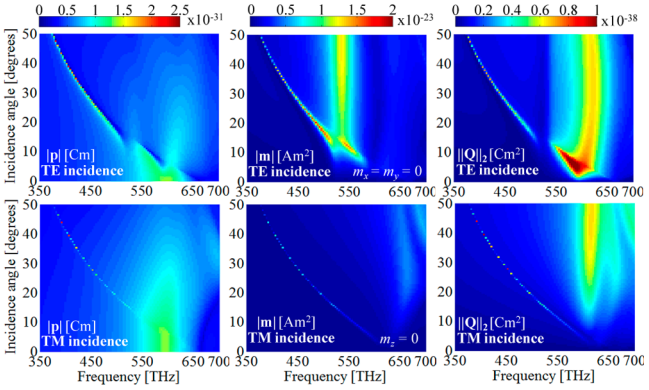

Figure 4. Strengths of electric dipole $|\mathbf{p}|$, magnetic dipole $|\mathbf{m}|$, and electric quadrupole $\|\underline{\mathbf{Q}}\|_2$ for the structure in Figure 3.

quadrupole $\|\underline{\mathbf{Q}}\|_2 = (\sum_{i=x,y,z}\sum_{j=x,y,z}|Q_{ij}|^2)^{1/2}$ in eq 5. Note that, when comparing TE and TM cases, $|\mathbf{p}|$ and $\|\underline{\mathbf{Q}}\|_2$ have similar strengths, whereas $|\mathbf{m}|$ is stronger in the TE case by about 1 order of magnitude. We also note that in the TE case $\mathbf{m}$ is purely along z, whereas in the TM case $\mathbf{m}$ has no z component, thus is only in-plane, as explicitly denoted in Figure 4 by mentioning the null components of $\mathbf{m}$. This is because the large cross-sectional area of the CNC on the $x-y$ plane results in a strong magnetic response under TE incidence. Note that some narrow features exhibiting peaks of $|\mathbf{m}|$ are accompanied with also sharp electric dipole and quadrupole contributions, though weaker in correspondence with magnetic Fano resonances, as it will be shown next.

To better emphasize the presence of array-induced and single-CNC-induced resonances, we plot in Figure 5 the

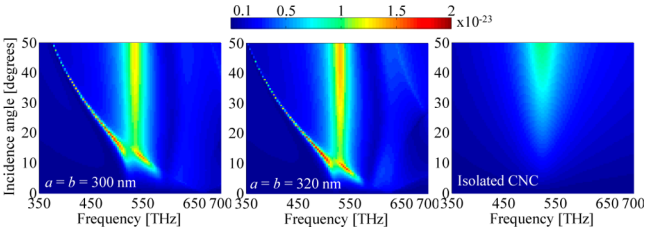

Figure 5. Strength of the magnetic dipole $|\mathbf{m}|$ in Am^2 under TE incidence for two metasurfaces with (a) $a = b = 300$ nm, (b) $a = b = 320$ nm, and (c) isolated CNC. The CNC design is as in Figure 3.

strength of the magnetic dipole $|\mathbf{m}|$ for the cases of metasurfaces with two different periods and isolated CNC. It is evident that the very narrow angular and spectral resonance appears only for metasurface cases and moves for varying periods, proving that it originates from the metasurface, and thus its nature is array-induced. On the other hand, the resonance at about 530 THz is mainly independent of array period and is a resonance pertaining to the CNC itself, as it appears also for an isolated CNC.

While the plot in Figure 4 quantitatively defines the contribution of each multipolar term to the optical properties and can for example be used to evaluate the radiated powers by each multipole as described in ref 48, it is still hard to conclude whether one is dominant or not. To this aim, we introduce three unitless parameters indicating how linear (L), circular (C), and mixed (M) the disposition of the N nanoparticles' electric dipole moments in the CNC is. Sketches explaining the meaning of the three parameters (L, C, M) are reported in the insets in Figure 6: linearity is a measure of dipole moments

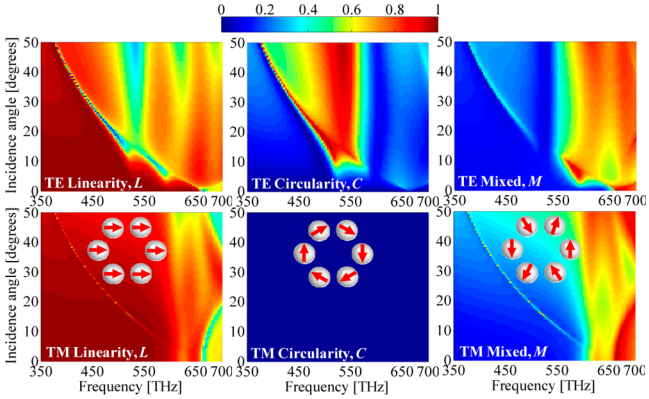

Figure 6. Linearity (L), circularity (C), and mixed state (M) pertaining to the result in Figure 3. Insets in bottom panels show the meaning of L, C, and M.

aligned in the same direction, C is the in-plane circularity of the dipole moments' disposition, and mixed includes all other possible configurations. These parameters are defined as

$$L = \frac{|\mathbf{p}_{\mathrm{lin,av}}|}{p_{\mathrm{mag,av}}}, \quad C = \frac{|p_{\mathrm{circ,av}}|}{p_{\mathrm{mag,av}}}, \quad M = \frac{p_{\mathrm{mixed,av}}}{p_{\mathrm{mag,av}}} \tag{6}$$

where the common normalization quantity is $p_{\mathrm{mag,av}} = (1/N)\sum_{i=1}^{N}|\mathbf{p}_i|$. Note that $p_{\mathrm{mag,av}}$ is evaluated at each frequency and incidence angle case, and therefore for this specific case by utilizing such a normalization scheme we obtain a measure of which one (ones) of the linear, circular, and mixed dipolar states dominates (dominate) the response of the cluster. Other parameters in eq 6 are given by (assuming the origin of the reference system at the center of the CNC in a unit cell)

$$\mathbf{p}_{\mathrm{lin,av}} = \frac{1}{N}\sum_{i=1}^{N}\mathbf{p}_i, \quad p_{\mathrm{circ,av}} = \frac{1}{N}\sum_{i=1}^{N}(\mathbf{p}_i - \mathbf{p}_{\mathrm{lin,av}})\cdot\hat{\boldsymbol{\varphi}}_i \tag{7}$$

with $\hat{\boldsymbol{\varphi}}_i = \hat{\mathbf{z}} \times \hat{\mathbf{r}}_i$, $\hat{\mathbf{r}}_i = \mathbf{r}_i/|\mathbf{r}_i|$, and

$$p_{\mathrm{mixed,av}} = \frac{1}{N}\sum_{i=1}^{N}|\mathbf{p}_i - \mathbf{p}_{\mathrm{lin,av}} - p_{\mathrm{circ,av}}\hat{\boldsymbol{\varphi}}_i| \tag{8}$$

We thus report color maps representing L, C, and M in eq 6 versus frequency and incidence angle in Figure 6 for case (ii) in Figure 2. We observe that while for TM incidence the dipolar state is mainly linear in the analyzed frequency and angular ranges (with some points with mixed polarization), for TE incidence a narrow feature (with respect to both frequency and incidence angle) induced by array effects is attributed mainly to a circular disposition of the electric dipole moments in the

dx.doi.org/10.1021/ph4001313 | ACS Photonics 2014, 1, 254−260

CNC: a magnetic Fano resonance. A single-CNC-induced magnetic resonance is also present around 530 THz, as proven by a peaking circularity. Again, note that narrow Fano resonances are also present under TM incidence; however this is out of the scope of this paper.

ENHANCED MAGNETIC AND ELECTRIC FIELDS AT THE FANO RESONANCE

In this section we are interested in the estimation of the magnetic and electric field enhancements. We make use of the information reported in Section IV to locate magnetic Fano resonances.

As a representative case, we plot in the top row of Figure 7 via the SDA method the magnetic and electric field

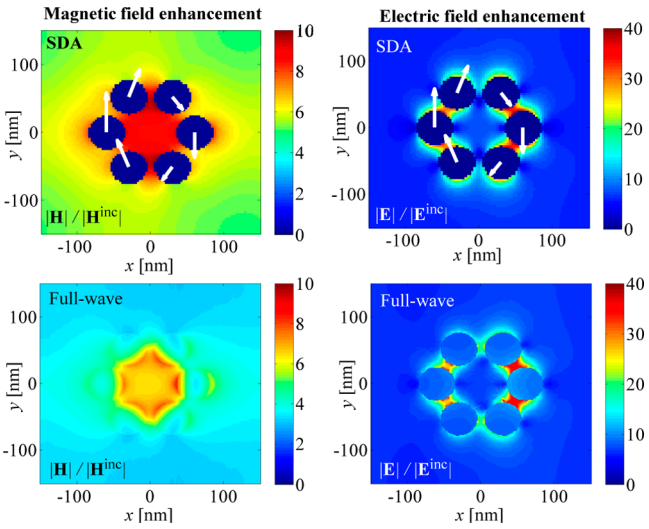

Figure 7. Magnetic and electric field enhancements in a unit cell in an $x-y$ plane cut at the array plane computed at a representative point of the magnetic Fano resonance marked as point 1 in the result in the top-left panel of Figure 3 for TE incidence. Top panels are computed via the SDA method (each nanoparticle's dipole moment direction is depicted with a white arrow). Only the field outside the nanoparticles is reported. Bottom panels are computed in correspondence with the full-wave simulation peak depicted by the thick dashed red curve in the bottom right plot of Figure 2 . Fields on the $x-y$ plane are reported.

enhancements in a unit cell in an $x-y$ plane cut at the array plane in correspondence with point 1 (the magnetic Fano resonance induced by array effects at 420.1 THz, 35 degrees, pertaining to the dashed red curve in the bottom right panel of Figure 2) explicitly indicated by a white arrow in Figure 3. We also plot white arrows that depict the electric dipole moment state of each nanoparticle in Figure 7. Their circulating disposition is a symptom of a magnetic resonance that results in a magnetic field enhancement of about 10 and an electric field enhancement of about 40. Furthermore, the magnetic field is spread over the large area of the CNC of nanoparticles. The electric field is instead mainly concentrated in the gaps between the nanoparticles. In the same figure's bottom row, we also plot the magnetic and electric field enhancements evaluated via full-wave simulations at the Fano resonance at 472 THz and 35 degrees for the case depicted by the thick dashed red curve in the bottom right plot of Figure 2. The full-wave simulation results show significant qualitative agreement with the SDA theory. For the same full-wave simulation setup, we plot in Figure 8 the volume current density in the particles composing

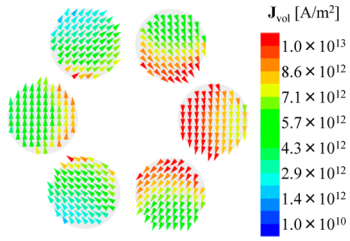

Figure 8. Volume current density in the particles composing the CNC computed via full-wave simulations for the case in the bottom row of Figure 7

the CNC computed as further proof of the magnetic resonance denoted by an evident circulating current density. Moreover, the higher order multipolar contributions in each nanoparticle's response (denoted by nonuniform current strengths inside the nanoparticles) is also visible in Figure 8, justifying the frequency shift observed in the bottom right panel of Figure 2 and the slight disagreement of the enhancement values shown in Figure 7.

We then plot in Figure 9 the magnetic field enhancement for the other three points indicated in the top-left panel of Figure 3

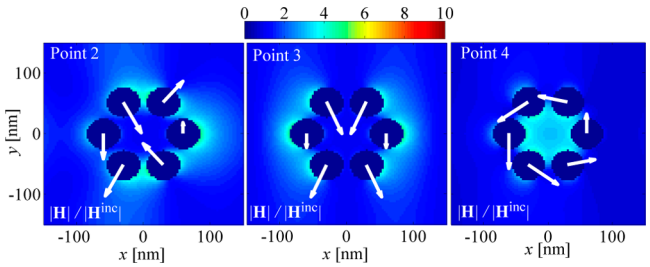

Figure 9. Magnetic field enhancement (computed via the SDA method) at the representative points 2, 3, and 4 indicated in the result in the top-left panel of Figure 3 for TE incidence.

to stress the importance of array-induced magnetic Fano resonances. At points 2 (600 THz, 5.5 degrees) and 3 (600 THz, 0 degrees), we observe a rather mixed and a rather linear disposition of the nanoparticles' dipole moments, respectively, in accordance with the results shown in Section IV. In these cases, the magnetic field enhancement is not spread over the CNC area and is smaller than the one reported in Figure 7, in contrast to the peculiar features observed in correspondence with magnetic Fano resonances. Indeed, at point 4 (533.8 THz, 50 degrees) we observe the circulating disposition of another (single-CNC-induced) magnetic resonance as it can also be inferred by the circularity plot in Section IV. Again the magnetic field is spread over the CNC area, with an enhancement of about 5. We stress again that a larger enhancement was achieved when using the array-induced magnetic Fano resonance, highlighting the importance of the metasurface analysis (instead of an isolated CNC) shown in this paper.

CONCLUSION

We have analyzed for the first time the possibility of exciting magnetic Fano resonances for the generation of enhanced magnetic and electric fields in metasurfaces made of CNCs of plasmonic nanoparticles. These are observed for oblique TE-polarized plane wave incidence illumination using both the SDA method and full-wave simulations. Interestingly, we have

dx.doi.org/10.1021/ph4001313 | ACS Photonics 2014, 1, 254−260

observed the presence of narrower angular and spectral array-induced resonances that lead to larger field enhancements than single-CNC-induced resonances, and this has not been suggested before. We have considered silver spherical nanoparticles as a representative case, although similar narrow resonances are expected for other nanoparticle geometries, such as nanodisks, and other materials, such as gold. In the latter case, higher plasmonic losses may affect the sharpness of the resonances. As shown in many previous investigations, and recently in ref 49 and references therein, large electric field enhancement in linear and triangular nanoparticle clusters requires the presence of very narrow gaps between nanoparticles. This in turn shows the powerfulness of magnetic resonances: with a gap of 10 nm, we are able to obtain a large electric field enhancement that could be used for surface-enhanced Raman spectroscopy applications (though this enhancement is available only in a narrow frequency/angular band when using CNCs). We further suggest that metasurfaces made of CNCs of plasmonic nanoparticles may be one of the building blocks for the development of innovative sensors based on enhanced magnetic fields as well as for the enhancement of magnetic nonlinearities.

AUTHOR INFORMATION

Corresponding Authors

*E-mail: scampion@uci.edu.
*E-mail: cguclu@uci.edu.
*E-mail: rragan@uci.edu.
*E-mail: f.capolino@uci.edu, http://capolino.eng.uci.edu/.

Notes

The authors declare no competing financial interest.

ACKNOWLEDGMENTS

This material is based upon work supported by the National Science Foundation under Grant No. CMMI-1101074. The authors thank Ansys Inc. for providing HFSS, which was instrumental in this work.

REFERENCES

(1) Pendry, J.; Holden, A.; Robbins, D.; Stewart, W. Magnetism from conductors and enhanced nonlinear phenomena. *IEEE Trans. Microwave Theory Tech.* **1999**, *47*, 2075−2084.

(2) Aydin, K.; Bulu, I.; Guven, K.; Kafesaki, M.; Soukoulis, C. M.; Ozbay, E. Investigation of magnetic resonances for different split-ring resonator parameters and designs. *New J. Phys.* **2005**, *7*, 168.

(3) Zhou, J.; Koschny, T.; Kafesaki, M.; Economou, E.; Pendry, J.; Soukoulis, C. Saturation of the magnetic response of split-ring resonators at optical frequencies. *Phys. Rev. Lett.* **2005**, *95*, 223902.

(4) Alù, A.; Salandrino, A.; Engheta, N. Negative effective permeability and left-handed materials at optical frequencies. *Opt. Express* **2006**, *14*, 1557−1567.

(5) Urzhumov, Y. A.; Shvets, G.; Fan, J. A.; Capasso, F.; Brandl, D.; Nordlander, P. Plasmonic nanoclusters: a path towards negative-index metafluids. *Opt. Express* **2007**, *15*, 14129−14145.

(6) Liu, N.; Fu, L.; Kaiser, S.; Schweizer, H.; Giessen, H. Plasmonic building blocks for magnetic molecules in three-dimensional optical metamaterials. *Adv. Mater.* **2008**, *20*, 3859−3865.

(7) Simovski, C. R.; Tretyakov, S. A. Model of isotropic resonant magnetism in the visible range based on core-shell clusters. *Phys. Rev. B* **2009**, *79*, 045111.

(8) Jeyaram, Y.; Jha, S. K.; Agio, M.; Löffler, J. F.; Ekinci, Y. Magnetic metamaterials in the blue range using aluminum nanostructures. *Opt. Lett.* **2010**, *35*, 1656−1658.

(9) Wheeler, M. S.; Aitchison, J. S.; Mojahedi, M. Coupled magnetic dipole resonances in sub-wavelength dielectric particle clusters. *J. Opt. Soc. Am. B* **2010**, *27*, 1083−1091.

(10) Vallecchi, A.; Albani, M.; Capolino, F. Collective electric and magnetic plasmonic resonances in spherical nanoclusters. *Opt. Express* **2011**, *19*, 2754−2772.

(11) Shafiei, F.; Monticone, F.; Le, K. Q.; Liu, X.-X.; Hartsfield, T.; Alu, A.; Li, X. A subwavelength plasmonic metamolecule exhibiting magnetic-based optical Fano resonance. *Nat. Nanotechnol.* **2013**, *8*, 95−99.

(12) Vallecchi, A.; Albani, M.; Capolino, F. Effect of irregularities of nanosatellites position and size on collective electric and magnetic plasmonic resonances in spherical nanoclusters. *Opt. Express* **2013**, *21*, 7667−7685.

(13) Sheikholeslami, S. N.; Alaeian, H.; Koh, A. L.; Dionne, J. A. A metafluid exhibiting strong optical magnetism. *Nano Lett.* **2013**, *13*, 4137−4141.

(14) Urban, A. S.; Shen, X.; Wang, Y.; Large, N.; Wang, H.; Knight, M. W.; Nordlander, P.; Chen, H.; Halas, N. J. Three-dimensional plasmonic nanoclusters. *Nano Lett.* **2013**, *13*, 4399−4403.

(15) Liu, N.; Mukherjee, S.; Bao, K.; Li, Y.; Brown, L. V.; Nordlander, P.; Halas, N. J. Manipulating magnetic plasmon propagation in metallic nanocluster networks. *ACS Nano* **2012**, *6*, 5482−5488.

(16) García-Cámara, B.; Gómez-Medina, R.; Sáenz, J. J.; Sepúlveda, B. Sensing with magnetic dipolar resonances in semiconductor nanospheres. *Opt. Express* **2013**, *21*, 23007−23020.

(17) Zhou, N.; Kinzel, E. C.; Xu, X. Complementary bowtie aperture for localizing and enhancing optical magnetic field. *Opt. Lett.* **2011**, *36*, 2764−2766.

(18) Shen, Q.; Hou, B.; Chen, Z.; Wang, Z.-L. Effect of gap width on enhanced magnetic optical fields in metallic split ring resonators. *AIP Adv.* **2012**, *2*, 042175−042178.

(19) Liu, H.; Sun, X.; Yao, F.; Pei, Y.; Huang, F.; Yuan, H.; Jiang, Y. Optical magnetic field enhancement through coupling magnetic plasmons to Tamm plasmons. *Opt. Express* **2012**, *20*, 19160−19167.

(20) Boudarham, G.; Abdeddaim, R.; Bonod, N. Enhancing magnetic near-field intensities with dielectric resonators. *arXiv:1303.4794v2*, 2013.

(21) Lorente-Crespo, M.; Wang, L.; Ortuño, R.; García-Meca, C.; Ekinci, Y.; Martínez, A. Magnetic hot spots in closely spaced thick gold nanorings. *Nano Lett.* **2013**, *13*, 2654−2661.

(22) Hong, Y.; Pourmand, M.; Boriskina, S. V.; Reinhard, B. M. Enhanced light focusing in self-assembled optoplasmonic clusters with subwavelength dimensions. *Adv. Mater.* **2013**, *25*, 115−119.

(23) Fan, J. A.; Wu, C.; Bao, K.; Bao, J.; Bardhan, R.; Halas, N. J.; Manoharan, V. N.; Nordlander, P.; Shvets, G.; Capasso, F. Self-assembled plasmonic nanoparticle clusters. *Science* **2010**, *328*, 1135−1138.

(24) Hentschel, M.; Dregely, D.; Vogelgesang, R.; Giessen, H.; Liu, N. Plasmonic oligomers: the role of individual particles in collective behavior. *ACS Nano* **2011**, *5*, 2042−2050.

(25) Ye, J.; Wen, F.; Sobhani, H.; Lassiter, J. B.; Dorpe, P. V.; Nordlander, P.; Halas, N. J. Plasmonic nanoclusters: near field properties of the Fano resonance interrogated with SERS. *Nano Lett.* **2012**, *12*, 1660−1667.

(26) Campione, S.; Guclu, C.; Ragan, R.; Capolino, F. Fano resonances in metasurfaces made of linear trimers of plasmonic nanoparticles. *Opt. Lett.* **2013**, *38*, 5216−5219.

(27) Liu, S.-D.; Yang, Y.-B.; Chen, Z.-H.; Wang, W.-J.; Fei, H.-M.; Zhang, M.-J.; Wang, Y.-C. Excitation of multiple Fano resonances in plasmonic clusters with D2h point group symmetry. *J. Phys. Chem. C* **2013**, *117*, 14218−14228.

(28) Miroshnichenko, A. E.; Flach, S.; Kivshar, Y. S. Fano resonances in nanoscale structures. *Rev. Mod. Phys.* **2010**, *82*, 2257−2298.

(29) Luk'yanchuk, B.; Zheludev, N. I.; Maier, S. A.; Halas, N. J.; Nordlander, P.; Giessen, H.; Chong, C. T. The Fano resonance in plasmonic nanostructures and metamaterials. *Nat. Mater.* **2010**, *9*, 707−715.

(30) Luk'yanchuk, B. S.; Miroshnichenko, A. E.; Yu, S. K. Fano resonances and topological optics: an interplay of far- and near-field interference phenomena. *J. Opt.* **2013**, *15*, 073001.
(31) Wu, C.; Khanikaev, A. B.; Adato, R.; Arju, N.; Yanik, A. A.; Altug, H.; Shvets, G. Fano-resonant asymmetric metamaterials for ultrasensitive spectroscopy and identification of molecular monolayers. *Nat. Mater.* **2012**, *11*, 69−75.
(32) Choi, J. H.; Adams, S. M.; Ragan, R. Design of a versatile chemical assembly method for patterning colloidal nanoparticles. *Nanotechnology* **2009**, *20*, 065301.
(33) Edwards, E. W.; Montague, M. F.; Solak, H. H.; Hawker, C. J.; Nealey, P. F. Precise control over molecular dimensions of block-copolymer domains using the interfacial energy of chemically nanopatterned substrates. *Adv. Mater.* **2004**, *16*, 1315−1319.
(34) Henzie, J.; Andrews, S. C.; Ling, X. Y.; Li, Z.; Yang, P. Oriented assembly of polyhedral plasmonic nanoparticle clusters. *Proc. Nat. Acad. Sci.* **2013**, *110*, 6640−6645.
(35) Klein, M. W.; Enkrich, C.; Wegener, M.; Linden, S. Second-harmonic generation from magnetic metamaterials. *Science* **2006**, *313*, 502−504.
(36) Rose, A.; Huang, D.; Smith, D. R. Demonstration of nonlinear magnetoelectric coupling in metamaterials. *Appl. Phys. Lett.* **2012**, *101*, 051103.
(37) Campione, S.; Guclu, C.; Ragan, R.; Capolino, F. Substrate Effects onto Complex Modes and Optical Properties of 2D Arrays of Linear Trimers of Plasmonic Nanospheres. In *Metamaterials Congress*; IEEE: Bordeaux, France, 2013.
(38) Bohren, C. F.; Huffman, D. R. *Absorption and Scattering of Light by Small Particles*; Wiley: New York, 1983.
(39) Steshenko, S.; Capolino, F. Single Dipole Approximation for Modeling Collections of Nanoscatterers. In *Theory and Phenomena of Metamaterials*; Capolino, F., Ed.; CRC Press: Boca Raton, FL, 2009; p 8.1.
(40) Steshenko, S.; Capolino, F.; Alitalo, P.; Tretyakov, S. Effective model and investigation of the near-field enhancement and subwavelength imaging properties of multilayer arrays of plasmonic nanospheres. *Phys. Rev. E* **2011**, *84*, 016607.
(41) Palik, E. *Handbook of Optical Constants of Solids*; Academic Press: New York, 1985.
(42) Draine, B. T. The discrete-dipole approximation and its application to interstellar graphite grains. *Astrophys. J.* **1988**, *333*, 848−872.
(43) Draine, B. T.; Flatau, P. J. Discrete-dipole approximation for scattering calculations. *J. Opt. Soc. Am. A* **1994**, *11*, 1491−1499.
(44) Yang, W.-H.; Schatz, G. C.; Van Duyne, R. P. Discrete dipole approximation for calculating extinction and Raman intensities for small particles with arbitrary shapes. *J. Chem. Phys.* **1995**, *103*, 869−875.
(45) Hessel, A.; Oliner, A. A. A new theory of Wood's anomalies on optical gratings. *Appl. Opt.* **1965**, *4*, 1275−1297.
(46) Auguié, B.; Barnes, W. L. Collective resonances in gold nanoparticle arrays. *Phys. Rev. Lett.* **2008**, *101*, 143902.
(47) *HFSS*, Finite element based simulation software; Ansys, 2013, http://www.ansoft.com/products/hf/hfss/.
(48) Jackson, J. D. *Classical Electrodynamics*; Wiley: New York, 1999.
(49) Campione, S.; Adams, S. M.; Ragan, R.; Capolino, F. Comparison of electric field enhancements: linear and triangular oligomers versus hexagonal arrays of plasmonic nanospheres. *Opt. Express* **2013**, *21*, 7957−7973.